Supporting information

Robust binding between secondary amines and Au electrodes

Weiyi Guo[a], Timothy Quainoo[b], Zhen-Fei Liu[b], Haixing Li[a,*]

[a]Department of Physics, City University of Hong Kong, Kowloon 999077, Hong Kong SAR, China
[b]Department of Chemistry, Wayne State University, Detroit, Michigan 48202, United States
*Corresponding author: haixinli@cityu.edu.hk

Table of content

I. General information

All compounds used in this study are commercially available and used without any further purification. **1** was purchased from Leyan (98%) and Energy (97%). **2** was purchased from Macklin (98%). **3** was purchased from Macklin (98%) and Leyan (98%). 1,2,4-Trichlorobenzene (TCB; anhydrous, $\geq$ 99%) and propylene carbonate (PC; suitable for HPLC, 99.7%) were purchased from Aladdin. Isopropanol (IPA; $\geq$ 99.7%) was purchased from Anaqua.

II. Scanning tunneling microscope-break junction experiment details

Single molecule conductance measurements were performed using a custom-built scanning tunneling microscope-break junction (STM-BJ) technique that has been described previously.[1, 2] A gold slug (Ø = 6 mm, 99.99-99.999%, Shijiazhuang Huake Metal Materials Technology Co. Ltd.) was mechanically polished, sonicated in an ultrasonic bath of isopropanol for 10 min, and was treated with UV-Ozone (UV Ozone cleaner L2002A2-UK, Ossila Limited, Sheffield, UK) for 20 min prior to use as the STM substrate. A freshly cut or a wax-coated Au wire (Ø = 0.25 mm, 99.999%, Hebei Hongju Metal Materials Co. Ltd) was used as the STM tip. For preparing a wax-coated Au tip, we followed a previously published method.[3] We started by melting Apiezon wax (Model W, M&I Materials Limited, Manchester, UK) on a 1.5 mm thick copper plate that was heated through a soldering iron element to 200°C. We then brought a freshly cut Au wire from underneath the plate and slowly raised it into the melted wax through a 1 mm wide slot in the copper plate, allowing it to uniform wetting. We continued to raise it through the wax until it broke the top surface of the melted wax. Finally, we moved the insulated tip sideways out of the plate, leaving the very end of the tip unperturbed. In conductance measurements under dry condition, we added 1mM concentration solution of molecule **1** in IPA on top of a prepared Au slug, dried the Au slug under ambient environment, and then brought the Au slug in contact with the wax-coated tip.

A commercially available single-axis piezoelectric positioner (P-840.10, Physik Instrumente (PI) GmbH & Co. KG, Karlsruhe, Germany) was used to achieve sub-angstrom level control of the tip-substrate distance. A variable gain low noise transimpedance current amplifier (DLPCA-200, FEMTO Messtechnik GmbH, Berlin, Germany) was used to record the current. The STM was controlled using a custom written program in IgorPro (Wavemetrics, Inc., OR, the United States) and operated in ambient conditions under room temperature. Solutions of 1 mM target molecules in TCB or PC were dropped onto the substrate for molecular conductance measurements. The tip was displaced at a speed of 30 nm/s and the current and voltage data were acquired at 40 kHz acquisition rate for all measurements. In this technique, we bring the Au STM tip into and out of contact with the substrate repeatedly while recording the conductance (current/voltage) of the junction. The conductance-displacement traces exhibit plateaus at integer multiples of the conductance quantum ($G_0 = 2e^2/h$) and the plateau at 1 G_0 corresponds to the formation of a single Au-Au atomic contact. After adding a solution of the target molecule, we observe plateaus in the conductance-displacement traces below 1 G_0 that we ascribe to the formation of an Au-molecule-Au junction after the single Au-Au contact was ruptured. For each measurement, we collected 3200 – 20000 traces to create 1D and 2D histograms without any data selection.

We use the following method for reporting the junction elongation length: we create 1D line profiles by integrating all counts in the 2D conductance histograms along the displacement axis and

obtain the junction elongation length by locating where the line profile drops to 20% of its peak intensity.
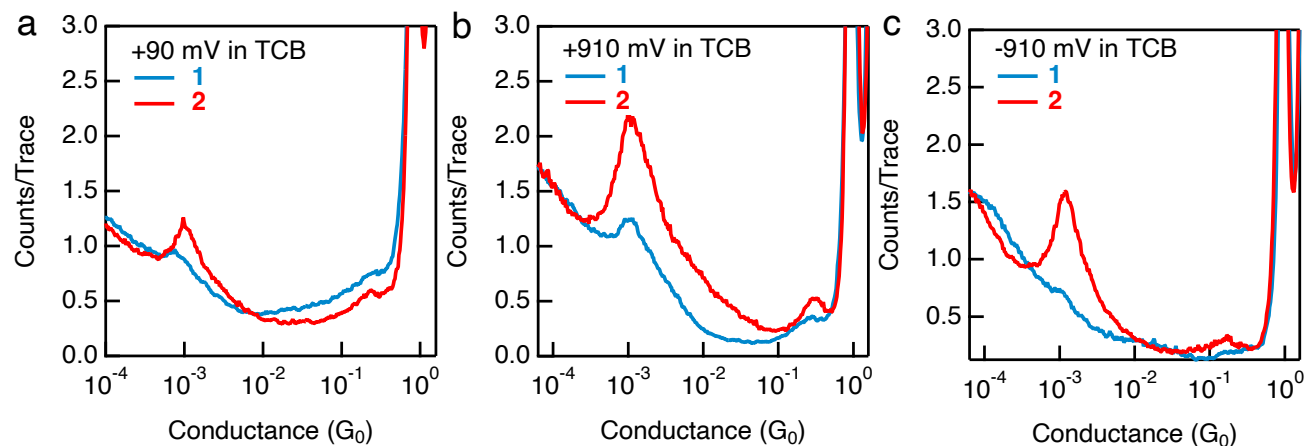
III. Additional figures

a +90 mV in TCB — 1 — 2

b +910 mV in TCB — 1 — 2

c -910 mV in TCB — 1 — 2

Axes: Counts/Trace vs Conductance (G_0)

Figure S1. 1D conductance histograms of **1** and **2** measured in TCB under (a) 90 mV, (b) 910 mV and (c) -910 mV tip bias.

a 1 in TCB +90 mV

b 1 in TCB -910 mV

c 1 in TCB +910 mV

d 2 in TCB +90 mV

e 2 in TCB -910 mV

f 2 in TCB +910 mV

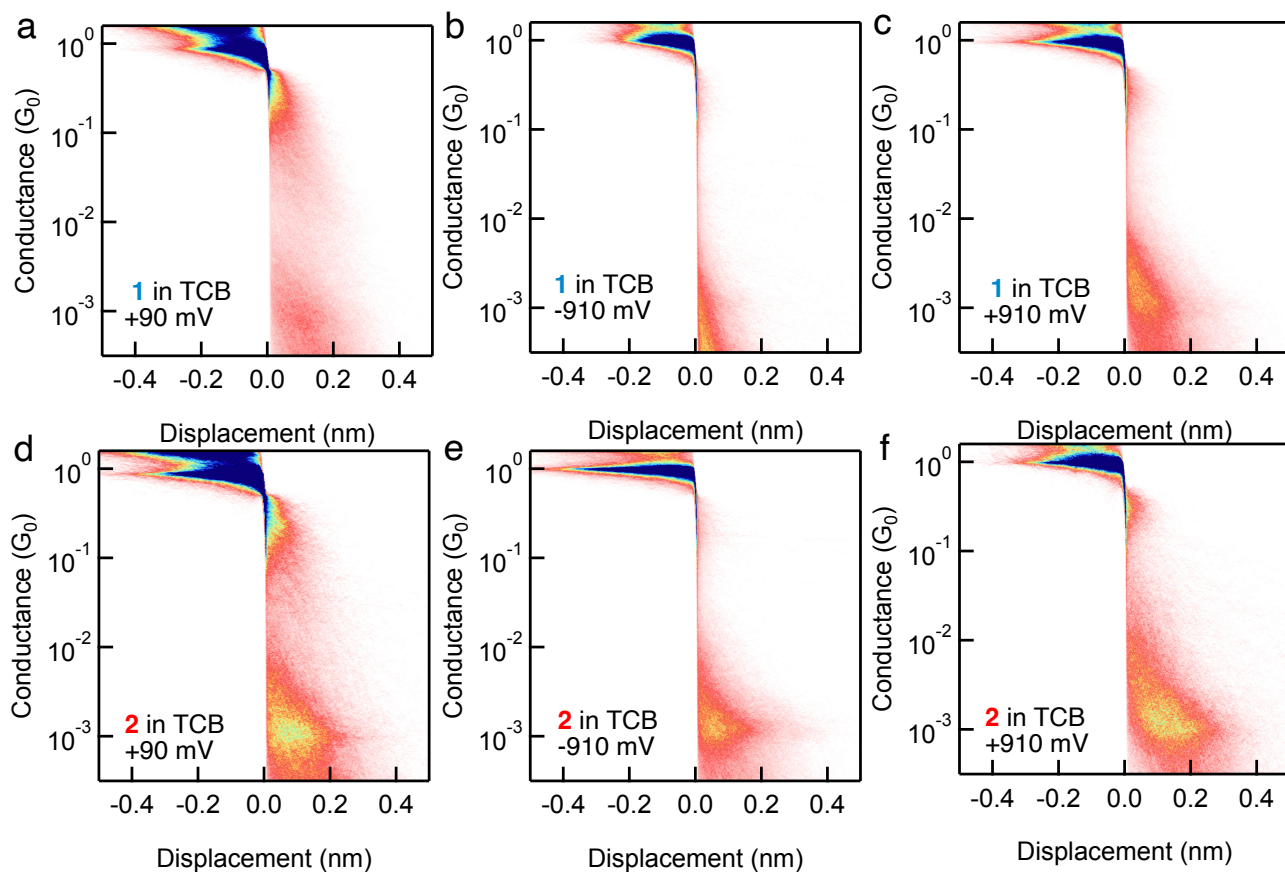*Axes: Conductance (G_0) vs Displacement (nm)*

Figure S2. 2D conductance histograms of (a)-(c) **1** and (d)-(f) **2** measured in TCB under 90 mV ((a) and (d)), -910 mV ((b) and (e)), and 910 mV ((c) and (f)) tip bias.
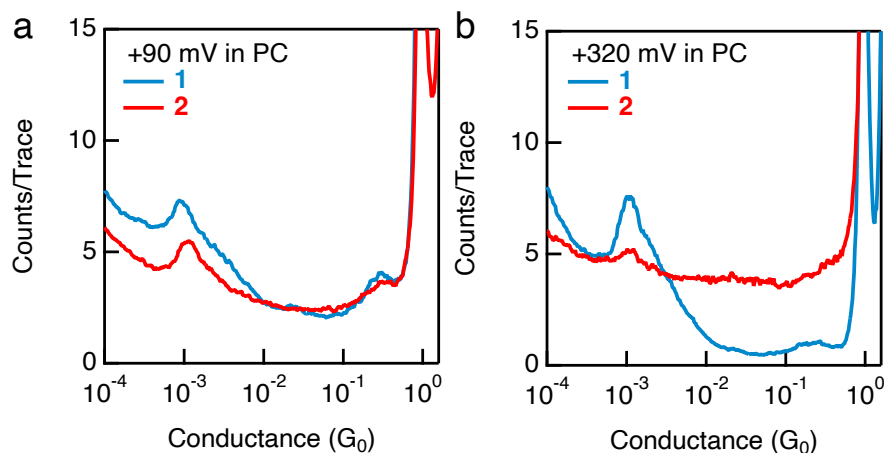
Figure S3. 1D conductance histograms of **1** and **2** measured in PC under (a) 90 mV and (b) 320 mV tip bias.
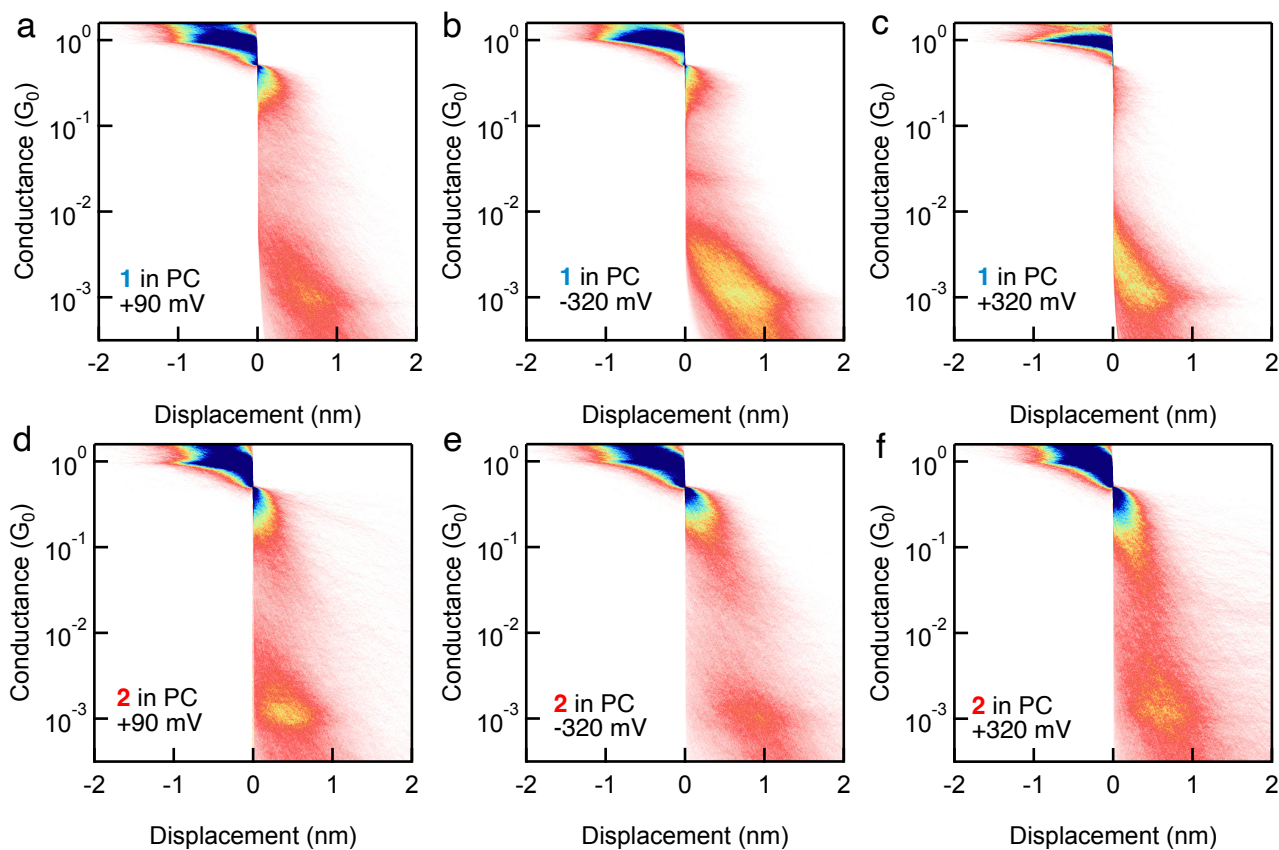

Figure S4. 2D conductance histograms of (a)-(c) **1** and (d)-(f) **2** measured in TCB under 90 mV ((a) and (d)), -320 mV ((b) and (e)), and 320 mV ((c) and (f)) tip bias.
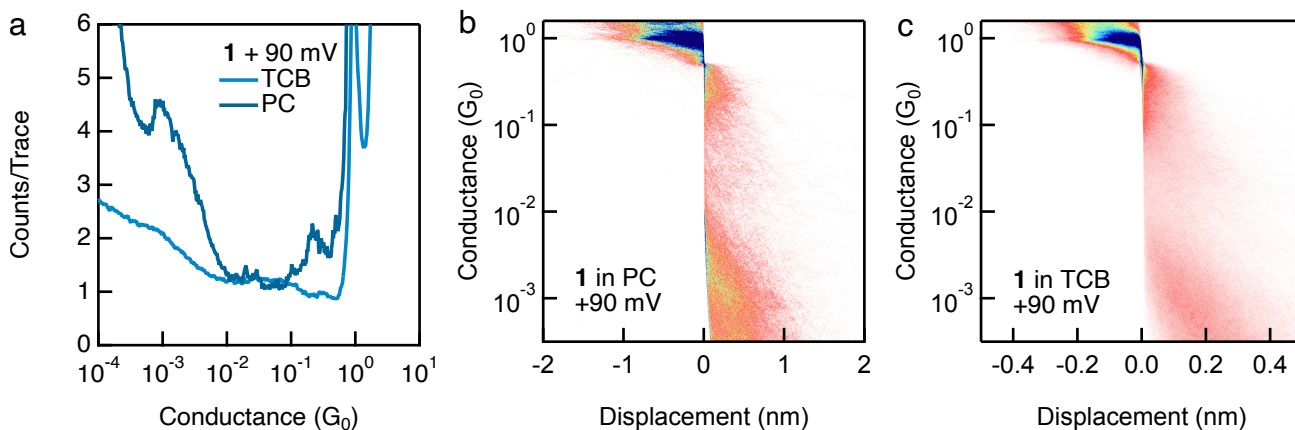
Figure S5. We purchase **1** from a different manufacturer Energy to check the reproducibility of this result, with all other measurements of **1** shown in this work performed on **1** purchased from Leyan. (a)1D conductance histograms of **1** measured in PC under 90 mV. 2D conductance histograms of **1** measured in (b) PC and (c) TCB under 90 mV.
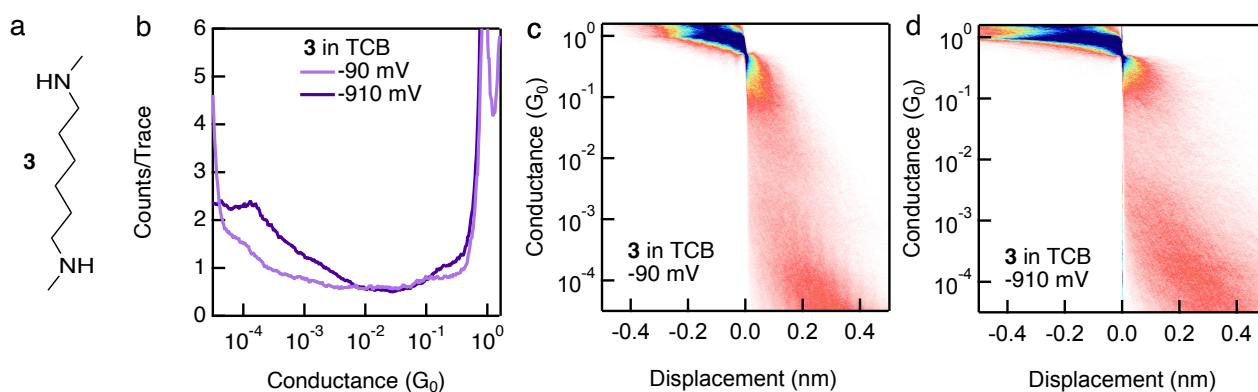

Figure S6. Conductance measurements of **3** purchased from Leyan in TCB with non-coated tip. (a) Chemical structure of **3**. (b) 1D conductance histograms of **3** measured in TCB under -90 mV and -910 mV tip bias. 2D conductance histograms of **3** measured in TCB under (c) -90 mV and (d) -910 mV tip bias.
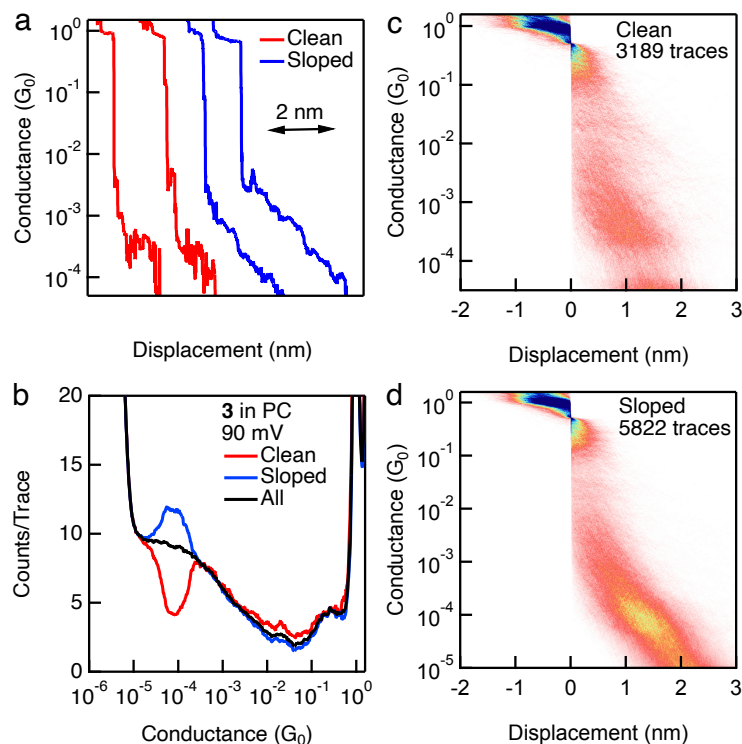
Figure S7. Conductance measurements of **3** purchased from Macklin in PC with wax-coated tip. (a) Example clean traces (red) and sloped traces (blue) of **3** measured in PC under 90 mV tip bias. (b) 1D conductance histograms generated from 3189 clean traces (red), 5822 sloped traces (blue) and all 9000 traces (clean and sloped traces combined, black). 2D conductance histograms generated from (c) 3189 clean traces and (d) 5822 sloped traces of **3** measured in PC under 90 mV.

Notes about **Figure S7**:

For the measurements of **3** with a wax-coated tip, we performed the measurement under a 90 mV tip bias and collected 9000 traces. We observed two types of traces in this measurement: the conductance traces that show a sharp drop in conductance from the molecular plateau to the noise level of the instrument (1×10^{-4} G_0), that we refer to as clean traces, and the conductance traces that show a sloped feature from molecular conductance to 1×10^{-4} G_0, which we refer to as sloped traces. Example clean and sloped traces are displayed in Supporting Information (SI) Figure S7a. Due to the significant presence of the sloped traces, the conductance histogram compiled from all traces does not show a well-defined conductance peak (black curve in SI Figure S7c).We therefore divide the total 9000 traces into two categories: 3189 clean traces and 5822 sloped traces, based on whether the trace demonstrates a sharp conductance drop from the molecular plateau to the noise level of the instrument, using an algorithm written in Igor. Our selection criteria ensures that we do not select conductance traces based on the value or length of the molecular conductance plateaus. We show 1D and 2D histograms generated from clean traces (red curve in Figure S7b and data in Figure S7c) and from sloped traces (blue curve in Figure S7b and data in Figure S7d). We observe a clear conductance peak at 3.1×10^{-4} G_0 in the histogram generated from clean traces, in agreement with the previous reported data for a hexane terminated with primary amine linker groups.[1, 4] This result agrees with what we observe in **1** and **2**: a same backbone terminated with primary amines, or with secondary amines, shows the same

single molecule conductance. Additionally, we find that the molecular plateau length is ~2 nm for **3** measured with a wax-coated tip, which is larger than the 1.78 nm molecular plateau length determined for **1**, in agreement with the longer distance between the two terminal groups for **3** than that of **1**.
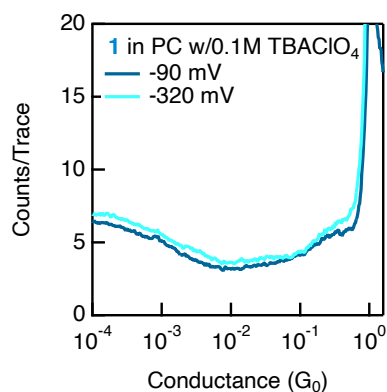

Figure S8. 1D conductance histograms of **1** measured in PC with 0.1 M TBAClO4 as supporting electrolyte under -90 mV and -320 mV tip bias.
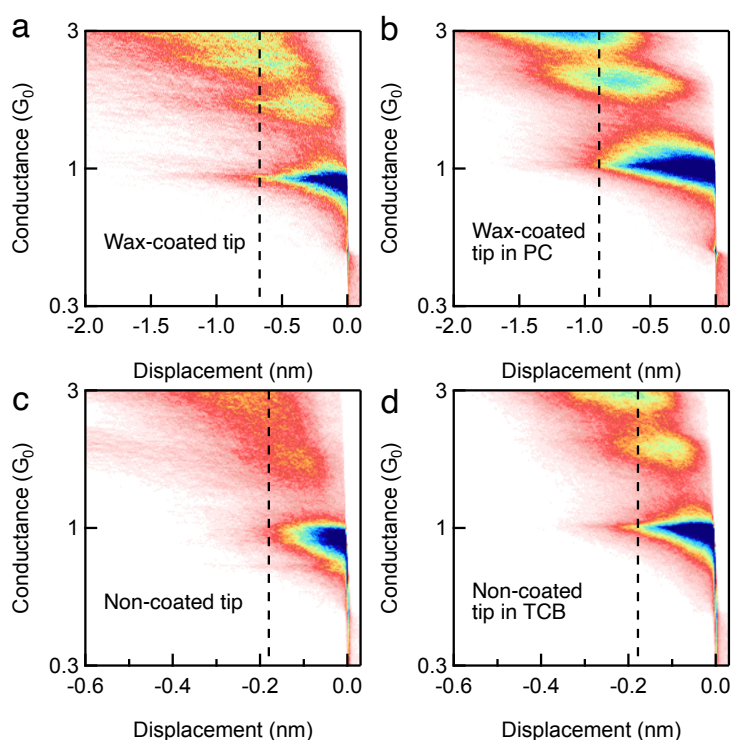

Figure S9. 2D conductance-displacement histograms (logarithmically binned using 100 bins/decade along the conductance axis) showing single Au—Au atomic contact signature (1 G_0) measured with a wax-coated tip in the (a) absence and (b) presence of PC (90 and -90 mV respectively) and measured with a non-coated tip in the (c) absence and (d) presence of TCB (-90 mV). Dashed lines indicate the Au—Au contact elongation length determined following methods described in SI Part II.
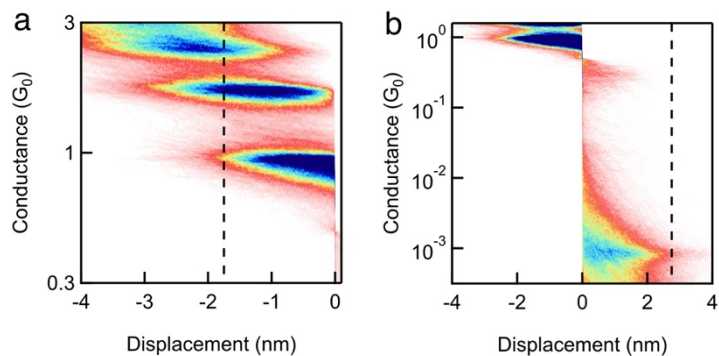
Figure S10. 2D histograms of **1** measured under dry condition with a 90 mV tip bias. 2D histograms of Au—Au contact and molecular junctions are displayed in (a) and (b), respectively. Dashed lines indicate the Au—Au atomic junction and molecular junction elongation length determined following methods described in SI Part II.
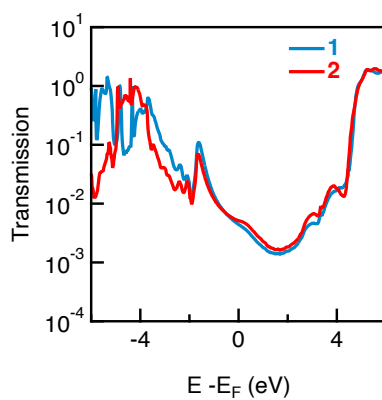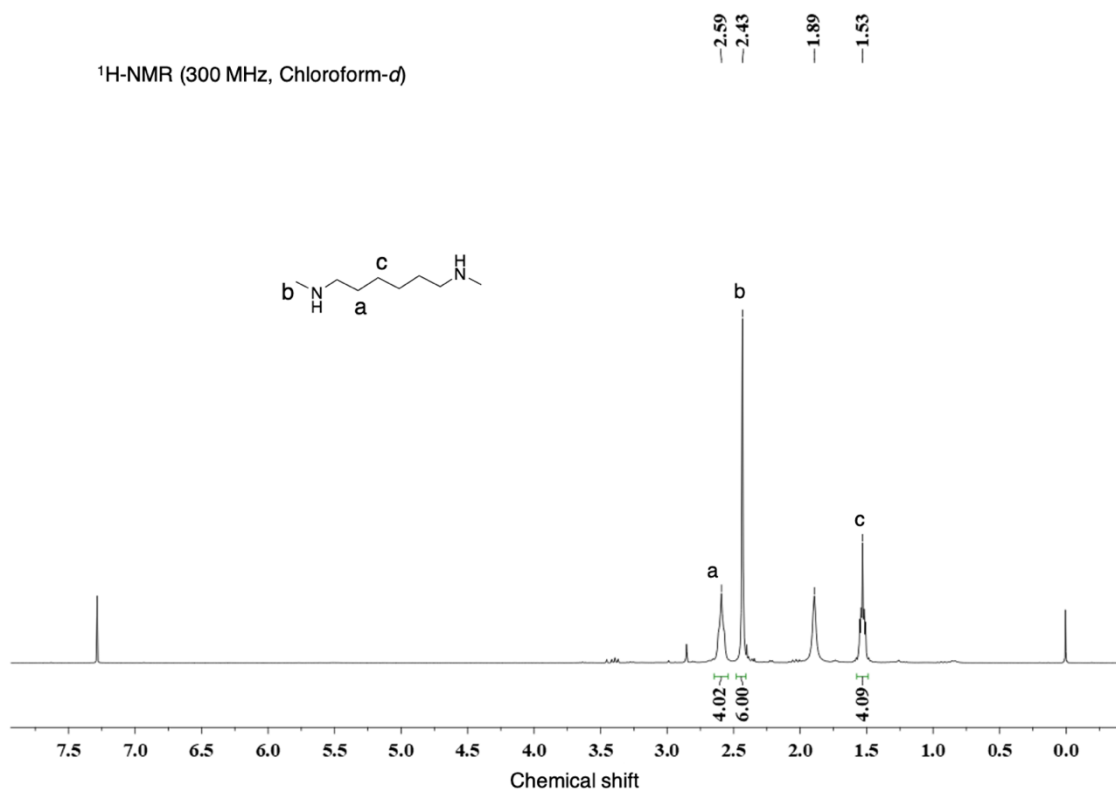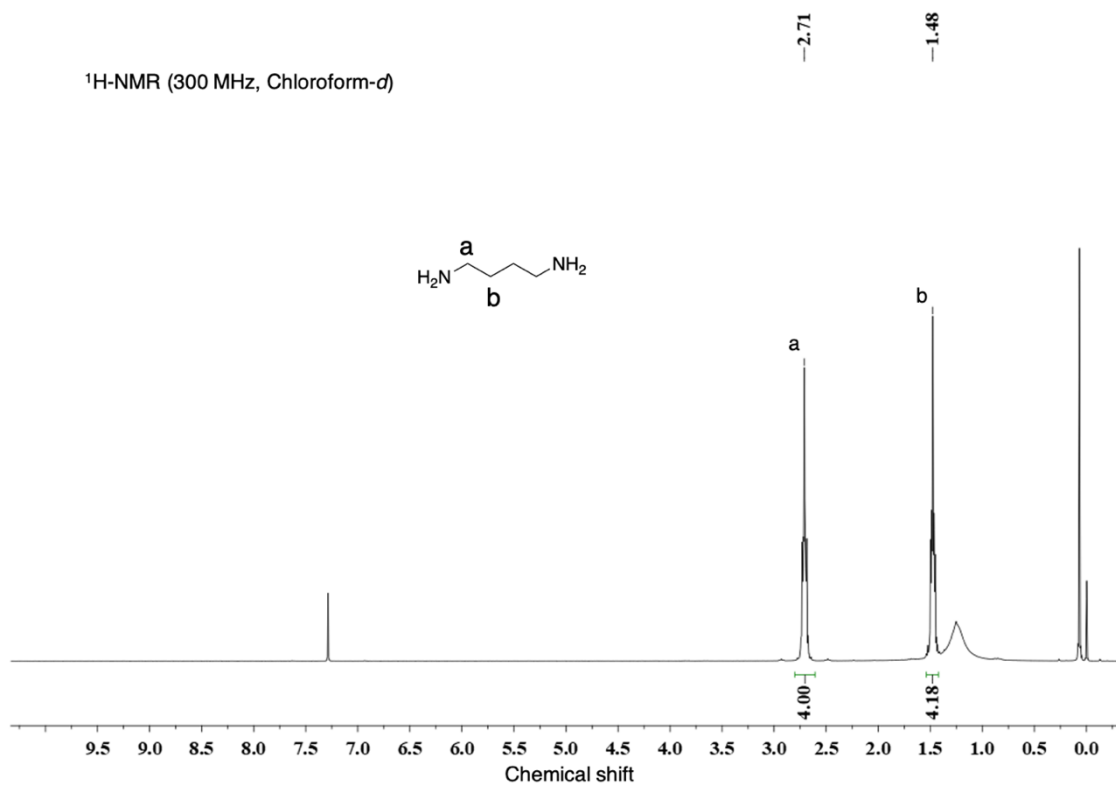

Figure S11. Transmission curves of **1** and **2** calculated from DFT.
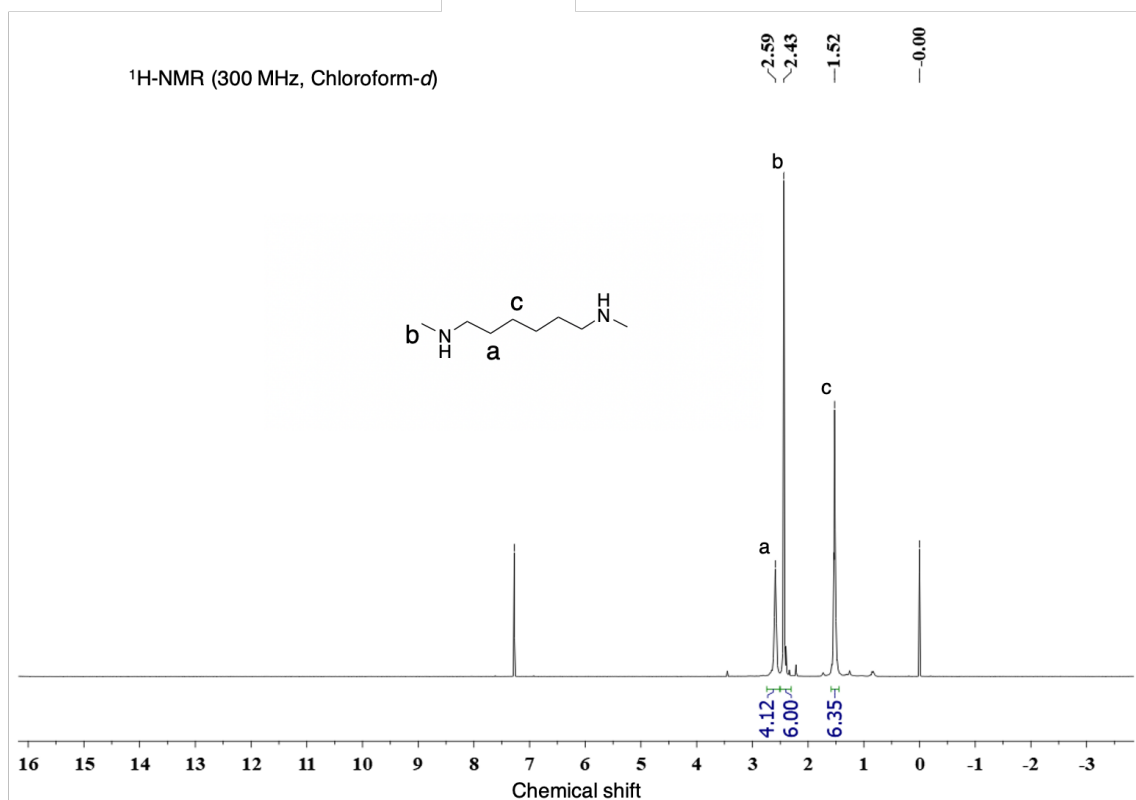
IV. ^{1}H-NMR Spectra

^{1}H-NMR of **1** purchased from manufacturer Leyan

^{1}H-NMR of **2** purchased from manufacturer Macklin

¹H-NMR of **1** purchased from manufacturer Energy

V. Computational details

For the binding energy calculations, the amine-Au interfaces are modeled by placing the primary or secondary amine molecule nearly vertically on Au (111) slabs with different Au binding motifs, as Figure 4 of the main text illustrates. Each Au slab consists of seven layers of Au (111) with 4×4 Au atoms on each layer. During the geometry optimizations, the lowest three layers of Au (111) are fixed, and the positions of all other atoms are fully relaxed until the residue forces are below 0.04 eV/Å. We use the Perdew-Burke-Ernzerhof (PBE) functional[5] as implemented in the SIESTA package,[6] a 4×4×1 **k**-mesh, single-zeta basis functions for Au that reproduce the work function of Au (111),[7] and double-zeta basis functions for other elements. After the interface structures are relaxed, the lowest three layers of Au (111) are removed. We then compute the total energy of the resulting interface, E(interface), the total energy of the Au slab (whose coordinates are fixed as those in the relaxed interface), E(slab), and the total energy of the molecule (whose coordinates are fixed as those in the relaxed interface), E(mol). For the calculation of the latter two quantities, ghost atoms are used to eliminate the basis set superposition error. The binding energy is then calculated using E(mol) + E(slab) − E(interface).

The supporting file coordinates.zip contains the Cartesian coordinates of the seven secondary amine-Au interface systems as shown in the Figure 4 of the main text, as well as the corresponding interfaces for the primary amines, in the .xyz file format. For all interfaces, the simulation cell is (the unit is Å):

11.935960	0.000000	0.000000
0.000000	10.336840	0.000000

0.000000   0.000000   50.000000

The primary and secondary amine molecular junctions are modeled by placing the molecule nearly vertically between two electrodes, with similar conformations as the aforementioned interfaces. Each electrode consists of seven layers of Au (111) with 4×4 Au atoms on each layer. The nitrogen atom in the amine group binds to an Au trimer, consistent with prior work.[8] During the geometry relaxations, the outmost three layers of Au (111) on either side are treated as a rigid body with the positions of all Au atoms in these layers fixed as in the Au bulk. The force acting on the outmost three layers is calculated as the average of all forces acting on the fourth layer. All inner four layers of Au (111) on both sides, the Au trimer on both sides, and all atoms in the molecule sandwiched between the two electrodes are allowed to fully relax until all forces are below 0.04 eV/Å. For the geometry optimization of the junctions, we use similar parameters as those used in the geometry optimization of the interfaces.

After the junction structures are relaxed, we perform PBE calculations with open boundaries to converge the non-equilibrium density matrix, as implemented in the TranSIESTA package.[9] Then we evaluate the Landauer formula non-self-consistently to obtain the transmission function T(E) at the PBE level. To quantitatively correct the energy level alignment in the junction to obtain a physical conductance value, we employ the DFT+Σ approach,[7, 10] following the recipe detailed previously.[11] The T(E) for the primary and secondary amine junctions calculated at DFT+Σ levels are shown in Figure 5 of the main text and at DFT levels are shown in Figure S11 in the supporting information.

VI. References

(1) Venkataraman, L.; Klare, J. E.; Tam, I. W.; Nuckolls, C.; Hybertsen, M. S.; Steigerwald, M. L. *Nano letters* **2006**, *6* (3), 458-462.

(2) Xu, B.; Tao, N. J. *science* **2003**, *301* (5637), 1221-1223.

(3) Nagahara, L.; Thundat, T.; Lindsay, S. *Review of scientific instruments* **1989**, *60* (10), 3128-3130.

(4) Chen, F.; Li, X.; Hihath, J.; Huang, Z.; Tao, N. *Journal of the American Chemical Society* **2006**, *128* (49), 15874-15881.

(5) Perdew, J. P.; Burke, K.; Ernzerhof, M. *Physical review letters* **1996**, *77* (18), 3865.

(6) Soler, J. M.; Artacho, E.; Gale, J. D.; García, A.; Junquera, J.; Ordejón, P.; Sánchez-Portal, D. *Journal of Physics: Condensed Matter* **2002**, *14* (11), 2745.

(7) Quek, S. Y.; Venkataraman, L.; Choi, H. J.; Louie, S. G.; Hybertsen, M. S.; Neaton, J. *Nano Letters* **2007**, *7* (11), 3477-3482.

(8) Zang, Y.; Pinkard, A.; Liu, Z. F.; Neaton, J. B.; Steigerwald, M. L.; Roy, X.; Venkataraman, L. *J Am Chem Soc* **2017**, *139* (42), 14845-14848.

(9) Papior, N.; Lorente, N.; Frederiksen, T.; García, A.; Brandbyge, M. *Computer Physics Communications* **2017**, *212*, 8-24.

(10) Neaton, J. B.; Hybertsen, M. S.; Louie, S. G. *Physical review letters* **2006**, *97* (21), 216405.

(11) Liu, Z.-F.; Wei, S.; Yoon, H.; Adak, O.; Ponce, I.; Jiang, Y.; Jang, W.-D.; Campos, L. M.; Venkataraman, L.; Neaton, J. B. *Nano letters* **2014**, *14* (9), 5365-5370.